Nano Energy 116 (2023) 108762

Contents lists available at ScienceDirect

Nano Energy

journal homepage: www.elsevier.com/locate/nanoen

Full paper

Electron transfer induced contact-electrification at oil and oleophobic dielectric interface☆

Huaifang Qin [a,b], Liang Xu [a,b,*], Fei Zhan [a,d], Zhong Lin Wang [a,c,*]

[a] Beijing Institute of Nanoenergy and Nanosystems, Chinese Academy of Sciences, Beijing 101400, PR China
[b] School of Nanoscience and Technology, University of Chinese Academy of Sciences, Beijing 100049, PR China
[c] Georgia Institute of Technology, Atlanta, GA 30332-0245, USA
[d] College of Chemical Engineering, Beijing University of Chemical Technology, Beijing 100029, PR China

ARTICLE INFO

Keywords:
Oil droplet
Contact-electrification
Fluid dielectric
Thermally stimulated current
Triboelectric nanogenerator

ABSTRACT

The oil dielectric has been used for enhancing the performance and durability of triboelectric nanogenerators (TENGs), but little is known about the contact-electrification (CE) (or triboelectrification) characteristics of the oil. Here, the CE behavior of different oil droplets with oleophobic surfaces is systematically investigated by dropping oil on a single-electrode TENG. The electrification trace is clearly imaged using a high-voltage scanning probe approach. Thermally stimulated discharge techniques are adopted for studying the detailed trapping characteristics of contact-generated charges with a homemade instrument, and the results are consistent with the thermionic emission model. The research provides systematic understandings on oil CE with oleophobic surfaces, together with general investigation paradigms and characterization methods for electrification phenomena on surfaces. Meanwhile, because typical oils are regarded as free of ions, their CE is attributed to electron transfer, which may contribute to the understanding of fundamental CE mechanisms.

1. Introduction

As an emerging technology for energy harvesting, triboelectric nanogenerators (TENGs) provide an effective solution of sustainable power supply for various distributed electronics that need to work wirelessly, from sensors of Internet of Things (IoT) to implantable medical devices [1–4]. They are also conceived to be aggregated massively to harvest power from wind or water waves, which can be large enough to contribute to the power grid [5–8]. TENGs work based on the coupling effect of triboelectrification and electrostatic induction, converting mechanical energy into electricity [9–12]. Before large-scale applications, challenges such as improving the power density and durability of the TENGs still need to be solved [13–15].

Traditionally, the structure of TENGs involves polymer layers and air as the dielectrics [16], and the latter as a fluid dielectric is often overlooked although important. Its characteristics of low dielectric strength, high moisture permeability, little lubrication effect and triboelectrification effect severely affect the performance of TENGs [17]. oil, as an alternative fluid dielectric, is extensively investigated recently for high-performance TENGs. Generally, the oil has a much higher dielectric strength, which is in favor of a larger static charge density on dielectric surfaces for improving power density [18–20]. The oil can provide a lubrication effect to enhance the durability of the TENGs [15], and it can protect the surface from water or water vapor that can severely impair most TENGs [21]. Moreover, the application of oil allows novel TENG designs based on fluidic interfaces, such as electric-double-layer nanogenerator [22]. For the above and other potential applications of oils in TENGs, the contact-electrification (CE) (or triboelectrification) characteristics of oils with solid surfaces are essential and crucial, which still lack systematic investigations. Meanwhile, because typical oils are regarded as free of ions, their CE can be attributed to electron transfer, which may contribute to the understanding of fundamental CE mechanisms [23–25].

In this paper, the CE behavior of oil droplets with oleophobic surfaces is systematically investigated by dropping oil on a single-electrode TENG. The electrification trace is clearly imaged with a high-voltage

☆ Prof Zhong Lin Wang, an author on this paper, is the Editor-in-Chief of Nano Energy, but he had no involvement in the peer review process used to assess this work submitted to Nano Energy. This paper was assessed, and the corresponding peer review managed by Professor Chenguo Hu, also an Associate Editor in Nano Energy

* Corresponding authors at: Beijing Institute of Nanoenergy and Nanosystems, Chinese Academy of Sciences, Beijing 101400, PR China.
E-mail addresses: xuliang@binn.cas.cn (L. Xu), zlwang@gatech.edu (Z.L. Wang).

https://doi.org/10.1016/j.nanoen.2023.108762
Received 9 July 2023; Received in revised form 31 July 2023; Accepted 3 August 2023
Available online 6 August 2023

scanning probe approach. Thermally stimulated discharge techniques are adopted for the first time to study the detailed trapping characteristics of contact-generated charges with a homemade instrument. The results provide systematic understandings on oil CE with oleophobic surfaces. The investigation paradigms and characterization methods developed here can also be used as general references for further researches on electrification phenomena of surfaces.

2. Results and discussion

2.1. Device structure and electrification process

The electrification experiments are conducted by dropping oil on a single-electrode TENG, which is regarded as a probe for studying liquid-solid interface charge transfer [26–28], as shown in Fig. 1a. The TENG is placed on a support frame with an incline angle of 11.5°, and the back electrode of the TENG is connected to the ground through an electrometer. A glass dropper is placed upon the TENG with a ground electrode at its lower end. The experiment involves a three-step process. The oil droplet first falls from the dropper to contact (or collide) with the TENG surface, then gradually rolls or slides to the lower end of the TENG, and finally leaves the TENG and falls into a sink. Fig. 1b demonstrates snapshots of the oil droplet falling from the dropper.

During the relative movement between the oil droplet and the TENG, the TENG surface is gradually electrified, and charge transfer from the back electrode as an effect of electrostatic induction can be observed. More specifically, the oil droplet falls and collides with the surface in the first step, and moves down in the second step. The different interaction manners produce two different electrified regions corresponding to the two steps respectively.

To ensure the oil droplet can move on the TENG surface with little residual oil, oleophobic surface is necessary, which is realized by a layer of fluorinated SiO_2 on the Kapton layer. Fig. 1c shows the scanning electron microscopy image of the TENG surface and the contact angle of the oil droplet (glycerol). Micro-structures are fabricated on the surface, and the glycerol droplet can achieve a contact angle of 136.4°. Contact angles of some other types of liquids are shown in Fig. S1. Fig. S2 presents detailed fabrication process of the TENG. In the experiments, glycerol is typically adopted (Fig. 1d). Other involved liquids include olive oil, squalane, tetradecane, castor oil and deionized (DI) water, and their dielectric constants and viscosities are listed in Table S1. Moreover, chemical groups in the oil molecules may be tuned to improve the output performance.

Fig. 1e shows detailed surface electrification process in the experiments. In the initial stage, there are few charges on the TENG surface, and the uncharged oil droplet falls to collide with the TENG surface as the first step. The oil droplet and the impact zone will be electrified with opposite charges due to the CE effect, and the surface is normally negatively charged [29]. Subsequently, in the second step, the oil droplet moves downward the surface with slighter interaction with the

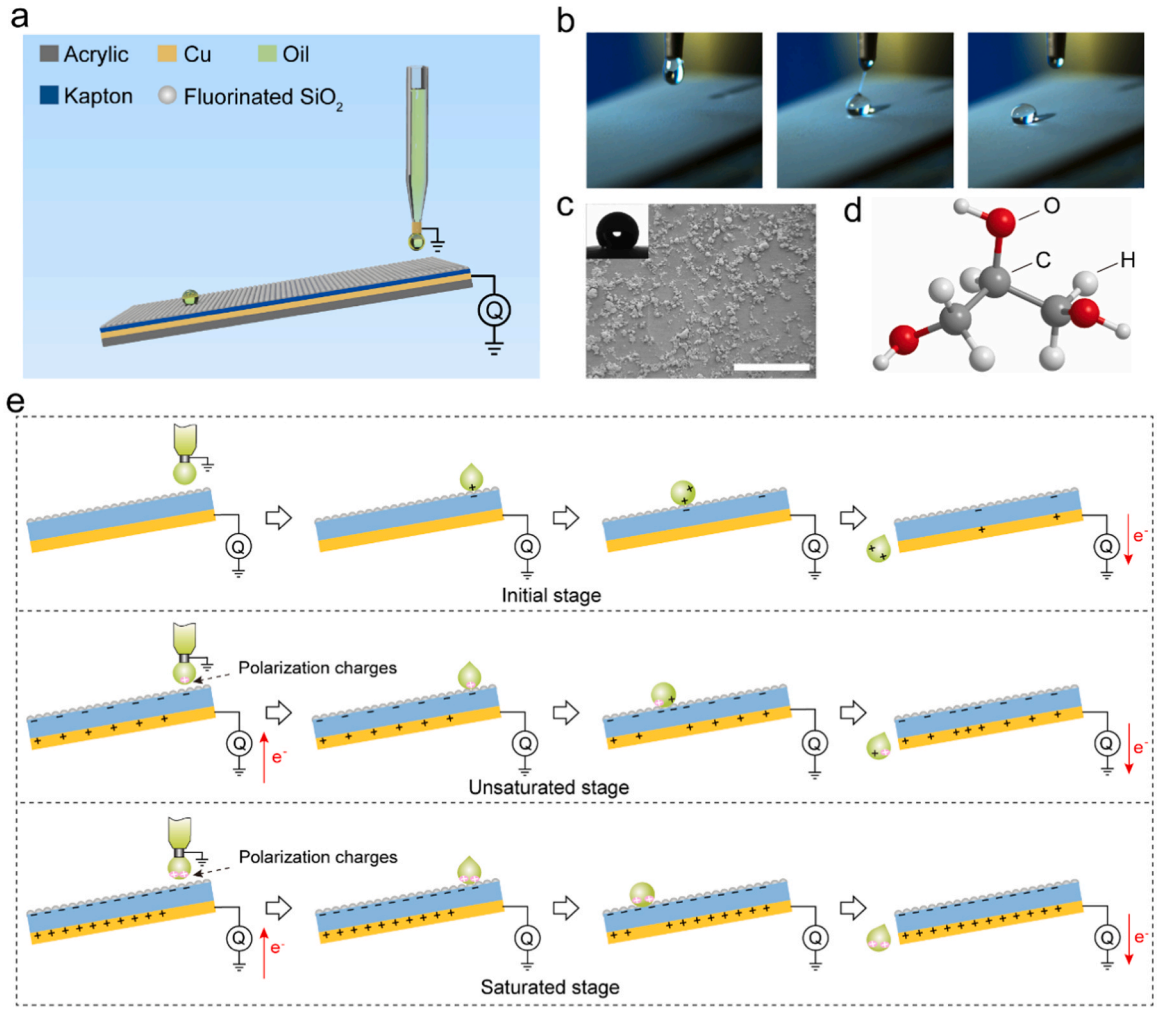

Fig. 1. Device structure and electrification process. (a) Schematic diagram of the electrification experiments. (b) Snapshots of the oil droplet falling from the dropper. (c) Scanning electron microscopy image of the TENG surface. Inset: contact angle of the oil droplet on the surface. Scale bar, 500 μm. (d) Molecular structure of glycerol. (e) Schematics of detailed surface electrification process in the experiments.

surface and is further electrified, which also gradually produce a negatively electrified trace on the surface. Finally, in the third step, the oil droplet falls from the lower end with positive charges, leaving negative charges on the TENG surface, which will cause the transfer of free electrons in the back electrode due to electrostatic induction [30]. In the unsaturated stage, as the TENG surface under the dropper is charged, the oil droplet will be polarized before its falling, which should be especially evident when the oil has a high dielectric constant and the dropper is very close to the surface. Thus, the falling droplet will take some positive charges before the contact, and causes opposite charge transfer in the back electrode in the first step. The droplet then moves along the surface with CE and finally leaves the surface with the polarization charges and contact-generated charges. With a series of droplets, the charges on the surface will get too crowd, and the surface may reach a saturated state, in which the oil droplet will only bear polarization charges and induce corresponding charge transfer in the back electrode.

2.2. Charge transfer characterization of the electrification experiments

The charge transfer from the back electrode is adopted to characterize the electrification process on the surface. According to the theory of single-electrode TENGs, there will be corresponding signals accompanying the motion of the oil droplet and the electrification process of the surface [26]. For example, there will be a step in the charge signal when a charged droplet falls on the surface from a distance and the step is equal to the charge amount of the droplet when the distance is large enough. When such a droplet leaves the surface to an enough distance, there will be an opposite step with the same height in the measured signal. However, in practical experiments, the distance is usually limited, so it is important to fix the configuration to make the results comparable. Fig. 2a presents the transferred charges from the back electrode in long-term oil dropping experiments, using glycerol and a dropping height of 0.5 cm, which are also typical experiment conditions afterward. It can be observed that the charge curve is mainly consisted of small downward and upward steps, corresponding to the falling down and leaving of the droplet, which are defined as contact charge Q_C and separation charge Q_S respectively. The total trend of the charge curve shows a saturation with rising number of oil droplets. Fig. S3a presents Q_C, Q_S and their difference. With the increase of oil droplet number, the value of Q_C gradually increases, while the value of Q_S first decreases and then increases, and the difference between Q_S and Q_C gradually approaches zero. According to the electrification process in Fig. 1e, the increase of Q_C should be attributed to the growing polarization of droplet by the enhancing electrification of the impact zone underneath, and the charge difference, which represents the charges taken away from the surface by the droplet, is reasonable to decrease, because with growing negative charges on the surface, it will be more difficult for the droplet to take positive charges away.

To more directly observe the electrification condition of the surface, a high-voltage scanning probe approach is developed, and the experiment setup is shown in Fig. S3b. Fig. S3c demonstrates preliminary images of the surface potential by the approach, which can be used to deduce the surface charge density that is linearly related to the surface potential [31]. It can be observed that after dropping oil, the motion trace of the oil droplet will be evidently electrified, and the impact zone has little difference with other electrified area. It should be noted that the coordinate here is related to the scanning range, which is not precisely aligned in different images. Fig. S3d shows a potential image of the complete trace after oil dropping where the ends of the electrode and the Kapton film can be seen. In the fabrication of the TENG, the Kapton

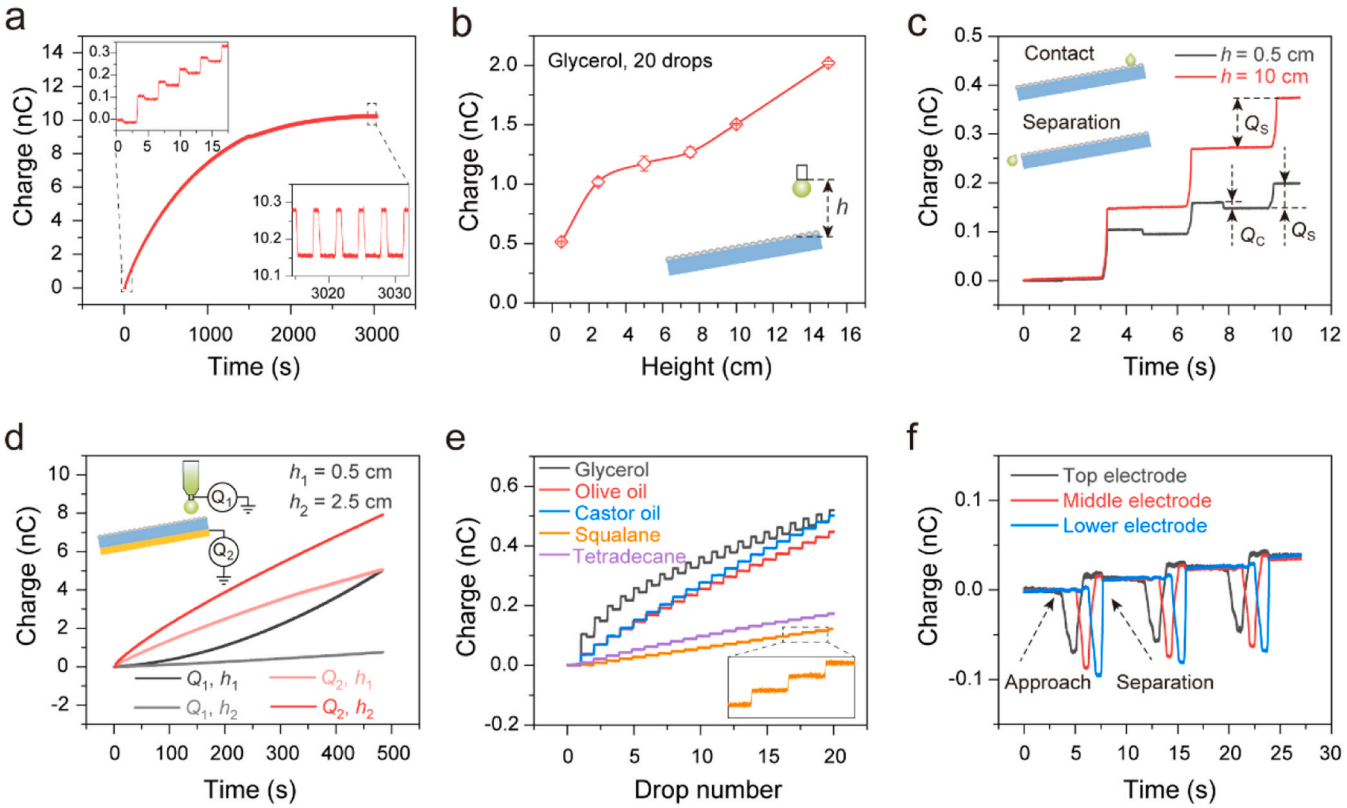

Fig. 2. Charge transfer characterization of the electrification experiments. (a) Transferred charges from the back electrode in long-term oil dropping experiments. (b) Dependence of total back-electrode transferred charges by 20 drops on the dropping height. Insert: schematic diagram of the dropping height. (c) Detailed curves of back-electrode transferred charges with different dropping heights. Insert: schematic diagram of contact and separation between the oil droplet and the TENG. (d) Transferred charges from the back electrode of the TENG and the ground electrode of the dropper. Insert: schematic diagram of charge testing. (e) Back-electrode transferred charges with different oils. (f) Transferred charges for arrayed back electrodes.

film is designed to be a bit larger than the electrode to avoid direct contact of the oil droplet with the back electrode. It can be observed that there is a zone with strong negative potential between the ends of the Kapton film and the electrode, which may be caused by the absence of free charges of the back electrode in the electrification. One may also notice that there is considerable potential value outside the film. This should be attributed to the resolution of the probe. Actually, the potential measurement is reliable only when there is a grounded back electrode, so the region on the electrode is mainly characterized afterward.

The dependence of total transferred charges on the dropping height h is shown in Figs. 2b and S4. The total back-electrode transferred charges by 20 drops increase almost linearly with the dropping height except small situations, and reach 2.02 nC for a height of 15 cm. To exclude the electrification effect of the droplet with air in the falling, the total charges of 10 droplets fallen in air from different heights were measured directly using a Faraday cup, showing neglectable charges (Fig. S5). Fig. 2c presents detailed comparison of back-electrode transferred charges with different dropping heights. For a small dropping height of 0.5 cm, there are evident steps of Q_C and Q_S, while the step of Q_C seems to disappear for a large dropping height of 10 cm, which can be attributed to that the surface charges at the impact zone cannot cause evident

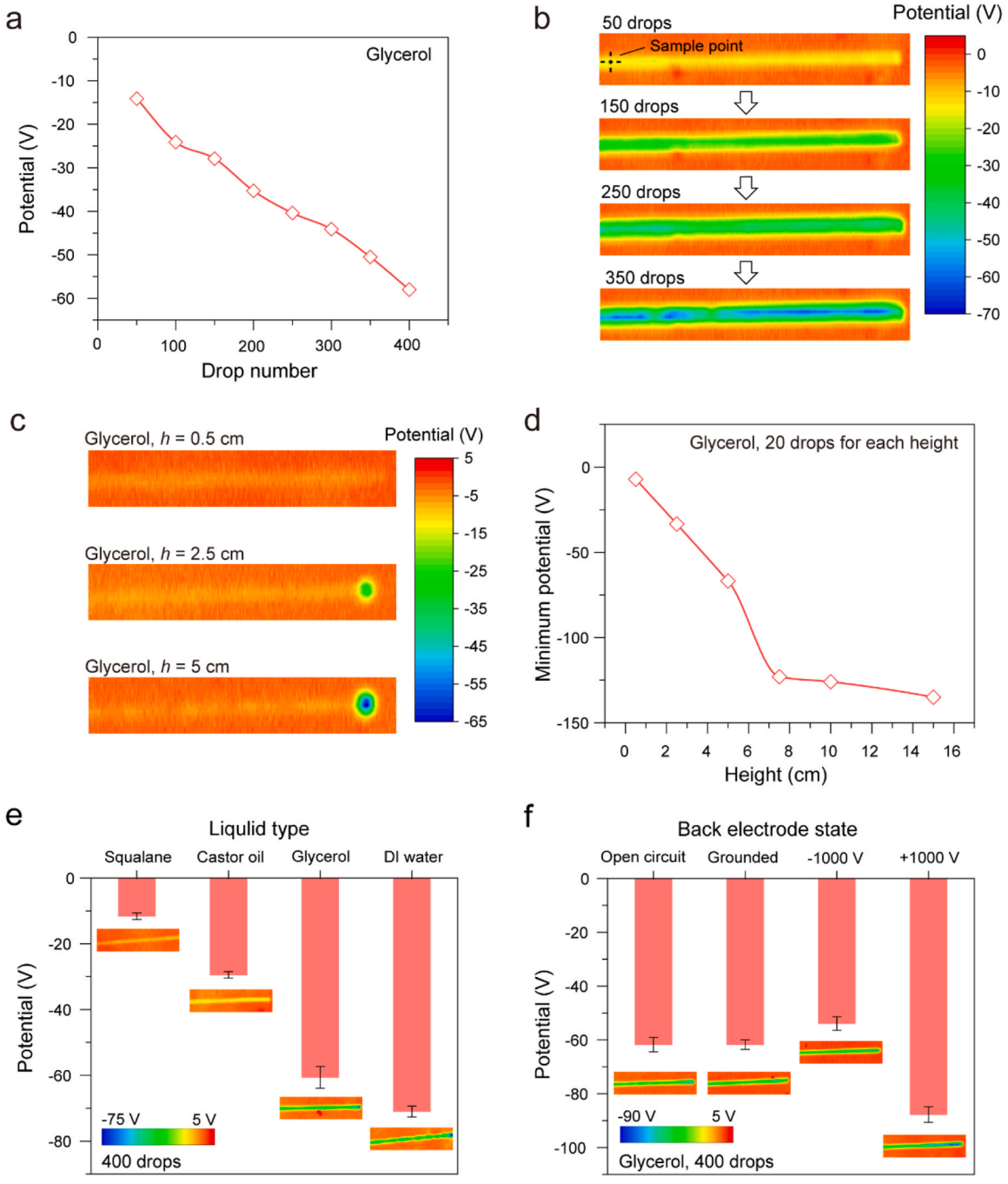

Fig. 3. Surface potential characterization of the electrification experiments. (a, b) Surface potential at the sample point (a) and potential images of the motion trace (b) for different numbers of oil droplets. (c, d) Potential images of the motion trace (c) and the minimum potential (d) for different dropping heights. (e) Surface potential with different types of liquids. Inset: potential images of the motion trace. (f) Surface potential with the back electrode in different states while dropping oil. Inset: potential images of the motion trace.

polarization on the droplet under a long distance, and the falling droplet will not bear evident polarization charges to cause a Q_C signal. The step of Q_C also can explain why the total charges for small h do not comply with the linear trend in Fig. 2b.

Fig. 2d and S6 provide more details on the polarization of the droplets. As described above, the positive polarization charges on the falling droplet will cause a signal in the back electrode. The corresponding negative polarization charges will be compensated through the ground electrode of the dropper, which are shown clearly in the figures and will also change to a small value with a large h. The corresponding steps in these two types of curves have almost the same value with opposite signs (Fig. S6).

Fig. 2e shows the transferred charges of different types of oils. For the oil with a low relative dielectric constant (Table S1), the polarization effect of oil droplets is weak, thus Q_C of olive oil, squalane, tetradecane, and castor oil is almost zero. The charge value for squalane is evidently low. Meanwhile, the difference of viscosity seems to have little effect on the transferred charges by comparing squalane and tetradecane.

To analyze the CE during the moving down of the droplet on the surface, the transferred charges for arrayed back electrodes were measured, as shown in Fig. 2f and S7. The charge steps, which correspond to the approach and separation of the droplet to each electrode, increase sequentially from the top electrode to the lower electrode, demonstrating gradually rising charge amount on the droplet while moving down the surface due to CE.

Besides, considering the charges have a long-range interaction, the influence of the detailed electrification experiment setup was also calibrated carefully. Fig. S8a shows schematic diagrams of two typical configurations. The back-electrode transferred charges with the two configures show evident difference (Figs. S8b-d). It is analyzed that the environment static charges, the shape of the grounded surface, and the shielding of fallen droplets etc. can all contribute to this difference. Thus, it is very important to fix the configuration carefully in such kind of experiments to control the unwanted influence. Here, the more compact configuration 2 is mainly adopted.

2.3. Surface potential characterization of the electrification experiments

Fig. 3a, b, and S9 present the electrification process of the TENG surface directly by measuring surface potential, which is linearly related to the surface charge density as discussed above. With the increase of the droplet number, the surface potential rises gradually, and the surface potential at the sample point shows linear relation with the drop number within 400 drops. Fig. 3c, d, and S10 show the surface potential with different dropping heights, where 20 drops of glycerol are dropped before imaging the potential. As shown in Fig. 3c, with increasing dropping height, the potential at the impact zone is gradually enhanced, showing a trap-like shape in the 3D image with growing area and rising depth (Fig. S10), and potential of other part of the motion trace shows little difference. This indicates that rising dropping height will mainly enhance the interaction at the impact zone by intensified collision. As shown in Fig. 3d, the minimum value of surface potential goes almost linearly with dropping height until 7.5 cm, where the slope gets gentler.

Fig. 3e shows the surface potential at the impact zone after dropping different kinds of liquid on the TENG surface. With 400 drops of each liquid, the sampled potential values for squalane, castor oil, glycerol, and DI water are − 11.61, − 29.44, − 60.63, and − 70.97 V, respectively. DI water demonstrates a stronger electrification capability at the impact zone in the experiment setup here. The low viscosity of water may enhance its contact with the surface when falling down.

The state of the back electrode during dropping can also affect the surface electrification. As shown in Figs. 3f and S11, whether the back electrode is open-circuited or grounded has no significant effect on the electrification, while applying a voltage can tune the electrification. When applying a − 1000 V voltage on the back electrode during oil dropping, the resulted surface potential at the impact zone will rise evidently, and a 1000 V voltage will result in a decrease for the potential, which means more negative charges are generated on the surface during electrification. The results imply that by altering the potential of the back electrode in the electrification, the electrified charges can be tuned.

2.4. Surface potential in thermally stimulated discharge experiments

In order to understand the characteristics of the above electrified charges on the TENG surface, thermally stimulated discharge experiments were conducted. Firstly, a simple setup shown in Fig. S12 is adopted, where the sample is placed directly on a heating table after oil dropping. To endure high temperature, the substrate is replaced by a piece of quartz plate in the sample fabrication. In the heating experiment, there is only a back electrode, with the upper surface exposed in air, which is similar to previous experiments by Lin et al. in microscale [32]. To better conduct the heat, the copper back electrode is designed to wrap the entire quartz plate.

In the experiments, the TENG was firstly dropped 400 glycerol droplets for electrification, then was placed on the heating table immediately. Fig. 4a and S13 show the variation of potential with heating time under different temperatures of isothermal heating. The potential was measured after the TENG being heated for 1, 2, 4, 8, and 12 min, respectively. Because the probe of the instrument cannot withstand high temperatures, the surface potential was measured at room temperature without in-situ measurement. The decay of surface potential is relatively slow at room temperature and it accelerates with rising temperature. With the heating temperature rising to 423 K, the potential decays much faster. Within 1 min, the potential decays from − 58.1 to − 12.1 V. Fig. 4b shows corresponding potential images by 423 K isothermal heating of different times, and the charges on the motion trace are basically eliminated after 8 min of heating. The decay of surface charges should be mainly caused by thermionic emission considering its exposure in air [23,32].

The TENG was also tested with linearly rising temperature of different ranges, using a rising rate of 3 K/min. Fig. 4c shows the variation of potential image under three temperature ranges, and Fig. 4d demonstrates transversely averaged potential over a width of 9 mm along the motion trace after the heating. When the temperature reaches 348 K, the surface charges are basically eliminated.

2.5. Thermally stimulated current measurement

To investigate more details of the charges on the surface, a delicate method of measuring thermally stimulated current (TSC) is adopted. The TSC has been widely used for studying charge trap characteristics of insulators and semiconductors, and related theories are well developed [33–36]. From the TSC spectrum, detailed information of trap depth and trap density can be calculated. In traditional TSC experiments, the sample is first polarized with high voltage, then depolarized with linearly rising temperature when the discharge current is monitored as the TSC [33–36]. Due to that the traps can be well filled with charges in the polarization stage, the TSC mainly reflects the trap information. For well crystallized materials, current peaks for discrete trap energy levels can be observed, and the peak temperature is related to the trap energy level and the peak height is related to the trap density [33–36]. For polymers that have complex structure, the distribution of trap energy levels can be quasi-continuous, and there will be no sharp peaks in the current signal. Compared with traditional TSC, the situation is a bit different here. Because the surface electrification is realized by friction or contact, the surface traps are not necessarily well filled, and the TSC mainly shows information of trapped charges. Considering that the TSC allows very detailed and precise calculation, the method should be very meaningful for investigating the mechanisms of CE.

Because commercial instruments for TSC only allows small-size samples, a homemade instrument is developed here and detailed

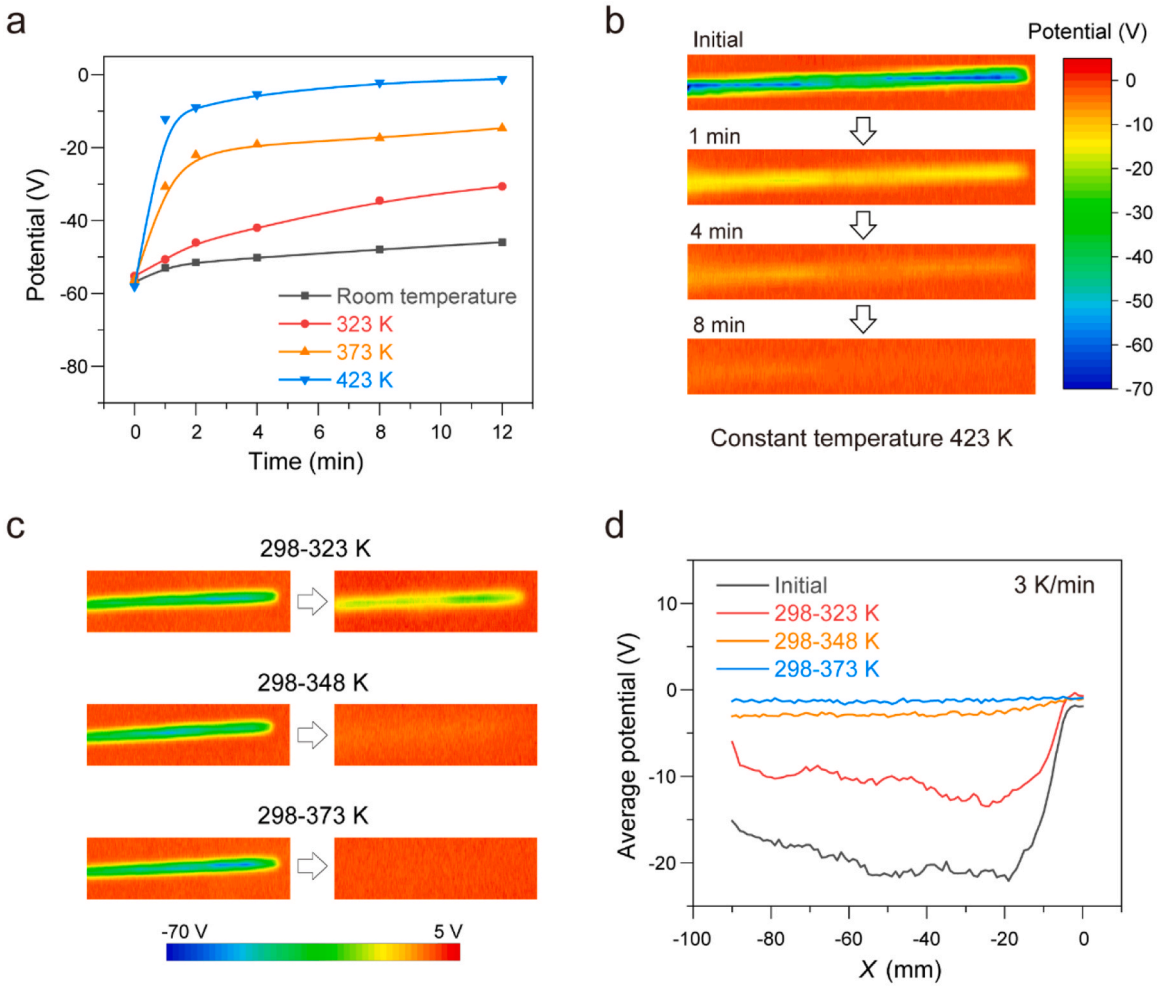

Fig. 4. Surface potential in thermally stimulated discharge experiments using a single-electrode configuration. (a) Decay of surface potential with isothermal heating in different temperatures. (b) Potential images of the motion trace with isothermal heating at 423 K. (c) Potential images of the motion trace heated by linearly rising temperature of different ranges. (d) Transversely averaged potential along the motion trace after the heating.

trapping characteristics of contact-generated charges on the surface are studied for the first time based on TSC. Fig. 5a shows the experiment setup which requires careful designs to measure tiny discharge current. A programmable heating table is used as the heating source under the sample, and the table is covered by an AlN plate with a size of 150 mm × 150 mm for insulation. A polished copper plate with a size of 100 mm × 50 mm × 1 mm is piled on the sample as the top electrode, and a gold layer of 80 nm is sputtered on both sides of the copper plate to prevent oxidation during heating. A piece of quartz plate is set upon the top electrode, with a mass of 1 kg above the quartz plate. A grounded Faraday cage is used to shield noise and stray signals. The preparation of the sample for TSC measurement is shown in Fig. S14. Because the temperature is not controlled with feedback, it was calibrated before the testing by comparing the measured and setting temperatures, as shown in Fig. S15. Before the TSC testing, the sample was mounted with the top electrode and the back electrode of the sample short-circuited, and was isothermally heated by a temperature of 473 K for 24 h to eliminate possible charges and initialize the sample.

In the experiments, firstly, the setup was verified by repeating discharging a sample with the same electrification condition. As shown in Fig. S16, the two measurements show good repeatability except small variations which may be attributed to the difference in electrification. Moreover, without charges on the surface, there will be no signal during the heating, as shown in the figure. It is also evident that after each heating process, the charges on the surface are eliminated, as shown in Fig. S16b. Here, due to the contact between the top electrode and the device surface, the fluorinated SiO_2 on the device surface partially falls off, so the potential images are slightly different. The above results prove that the setup is reliable for the TSC testing.

Fig. 5b shows the TSC for electrification conditions using different numbers of droplets. In the testing, the electrified sample was placed on the heating table, and waited until the current at the room temperature reduced to a value close to zero for releasing some very shallowly trapped charges on the surface. Then the sample was heated by linearly rising temperature from 298 to 423 K with a rising rate of 3 K/min. For the case with 400 drops, there is no sharp peaks in the TSC, which should be attributed to the complex trap energy level distribution on the sample surface as discussed above. The TSC reaches a maximum value of 2.75 pA at about 340 K, then starts to decrease, and drops to near zero at about 390 K. For the case with 200 drops, the maximum current decreases to 1.47 pA, indicating that the amount of trapped charges decreases obviously. The shape of the current curve for this case is not very regular, which may be attributed to very low filling condition of surface traps. The corresponding potential images are shown in Fig. S17.

Fig. 5c and d demonstrate the surface potential and variation of the TSC curve with different dropping heights. By raising the dropping height to 10 cm, the potential at the impact zone will rise significantly. The corresponding TSC reaches a maximum value of 4.88 pA at 340 K, where the TSC is about 2.2 pA for a dropping height of 0.5 cm. This indicates that the amount of trapped charges increases evidently with

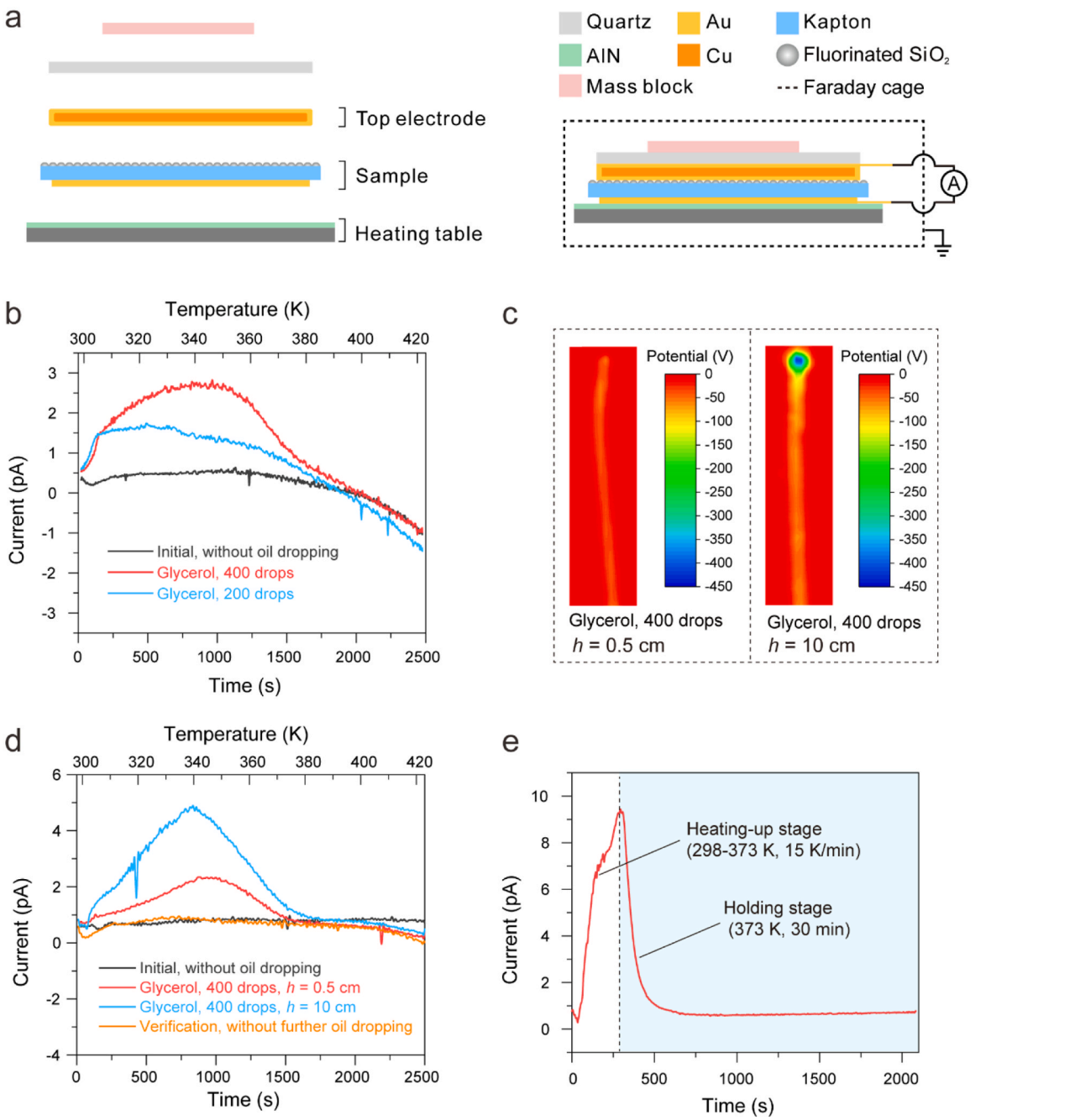

Fig. 5. Thermally stimulated current measurement. (a) Schematics of thermally stimulated current testing. (b) Thermally stimulated current with different numbers of oil droplets. (c, d) Initial surface potential (c) and thermally stimulated current (d) with different dropping heights. (e) Discharge current with isothermal heating at 373 K.

higher dropping height. The temperature for the maximum value of the 0.5 cm case seems to shift higher slightly, which may roughly imply that the proportion of charges trapped in higher energy levels (or deep traps) increases.

The discharge current can also be measured under a condition of isothermal heating. Fig. 5e shows the discharge current of a sample electrified with 400 glycerol drops under isothermal heating of 373 K. The temperature first rose fast from 298 to 373 K with a rising rate of 15 K/min, then was hold at 373 K for 30 min. A large discharge current of 9.3 pA is obtained when the temperature reaches 373 K, which decays fast subsequently in the isothermal heating. Fig. S18 shows corresponding images of surface potential.

Moreover, because oils are typically regarded as free of ions, the CE (or triboelectrification) of oils should depend on electron transfer. Considering the experiments here were conducted with high-purity oils, the above results can be mainly attributed to electron behavior, which may contribute to the understanding of fundamental CE mechanisms.

3. Conclusions

In this paper, the CE behavior of different oil droplets with oleophobic surfaces is systematically investigated by dropping oil on a single-electrode TENG. The transferred charges from the back electrode are measured to characterize the electrification process on the surface, and the surface potential is imaged directly using a high-voltage scanning probe approach. The influences of droplet number, dropping height

and oil type are investigated systematically. Thermally stimulated discharge techniques are adopted for the first time to study the detailed trapping characteristics of contact-generated charges with a homemade instrument. The research provides systematic understandings on oil CE with oleophobic surfaces, together with general investigation paradigms and characterization methods for electrification phenomena on surface. The results should also be very meaningful for the design of droplet TENGs [9,30].

4. Experimental section

4.1. Fabrication of the device for oil dropping

First, an acrylic substrate was cut by a laser cutter (PLS6.75) with dimensions of 100 mm × 50 mm × 3 mm. A copper electrode with a thickness of 30 μm was attached to the substrate as the back electrode. Then, a piece of Kapton film (3M, thickness: 50 μm) was attached on the copper electrode as the dielectric layer. Finally, a layer of fluorinated SiO_2 was sprayed on the surface of the Kapton film and dried at room temperature for 4 h.

4.2. Fabrication of the sample for TSC testing

First, a piece of Kapton film was cut with dimensions of 115 mm × 65 mm. Tapes with a width of 5 mm were stuck around the Kapton film as a mask. Then, a gold electrode with a thickness of 40 nm was sputtered to the Kapton film as the back electrode. Finally, the tapes were removed, and a layer of fluorinated SiO_2 was sprayed on the other side of the Kapton film and dried at room temperature for 4 h.

4.3. Characterization methods

The transferred charges and TSC were measured by an electrometer (Keithley 6517B). The charges of oil droplets fallen in air were measured by a Faraday cup (Monroe). The surface potential of the device was measured by an electrostatic voltmeter (Trek 347), and a 2D displacement platform (Zolix KSA100–11-X for each dimension) was used for scanning in the potential measurement. A source meter (Keithley 2410) was adopted as the voltage source. A 25 mL glass dropper was used for dropping oil. A programmable heating table (JW-400DG) was used for the heating tests.

CRediT authorship contribution statement

Liang Xu and Zhong Lin Wang conceived the idea. Liang Xu, Huaifang Qin, and Fei Zhan designed the device and experiments. Huaifang Qin fabricated the device and did the experiments. Liang Xu and Huaifang Qin discussed the data and prepared the figures. Liang Xu, Huaifang Qin, and Zhong Lin Wang wrote and revised the manuscript. Liang Xu and Zhong Lin Wang guided the project.

Declaration of Competing Interest

The authors declare that they have no known competing financial interests or personal relationships that could have appeared to influence the work reported in this paper.

Data availability

Data will be made available on request.

Acknowledgments

The research was supported by the National Key R & D Project from Minister of Science and Technology (2021YFA1201603, 2021YFA1201601), the Key Research Program of Frontier Sciences, CAS (ZDBS-LY-DQC025), the National Natural Science Foundation of China (51735001), and Youth Innovation Promotion Association, CAS (2019170).

Appendix A. Supporting information

Supplementary data associated with this article can be found in the online version at doi:10.1016/j.nanoen.2023.108762.

References

[1] F.R. Fan, Z.Q. Tian, Z.L. Wang, Flexible triboelectric generator, Nano Energy 1 (2012) 328–334.
[2] S. Wang, J. Xu, W. Wang, G.N. Wang, R. Rastak, F. Molina-Lopez, J.W. Chung, S. Niu, V.R. Feig, J. Lopez, T. Lei, S.K. Kwon, Y. Kim, A.M. Foudeh, A. Ehrlich, A. Gasperini, Y. Yun, B. Murmann, J.B. Tok, Z. Bao, Skin electronics from scalable fabrication of an intrinsically stretchable transistor array, Nature 555 (2018) 83–88.
[3] Z.L. Wang, From contact electrification to triboelectric nanogenerators, Rep. Prog. Phys. 84 (2021), 096502.
[4] D. Choi, Y. Lee, Z.H. Lin, S. Cho, M. Kim, C.K. Ao, S. Soh, C. Sohn, C. Jeong, J. Lee, M. Lee, S. Lee, J. Ryu, P. Parashar, Y. Cho, J. Ahn, I. Kim, F. Jiang, P.S. Lee, G. Khandelwal, S.J. Kim, H. Kim, H. Song, M. Kim, J. Nah, W. Kim, H. Menge, Y. Park, W. Xu, J. Hao, H. Park, J. Lee, D. Lee, S. Kim, J. Park, H. Zhang, Y. Zi, R. Guo, J. Cheng, Z. Yang, Y. Xie, S. Lee, J. Chung, I. Oh, J. Kim, T. Cheng, Q. Gao, G. Cheng, G. Gu, M. Shim, J. Jung, C. Yun, C. Zhang, G. Liu, Y. Chen, S. Kim, X. Chen, J. Hu, X. Pu, Z. Guo, X. Wang, J. Chen, X. Xiao, X. Xie, M. Jarin, H. Zhang, Y. Lai, T. He, H. Kim, I. Park, J. Ahn, N. Huynh, Y. Yang, Z.L. Wang, J. Baik, D. Choi, Recent advances in triboelectric nanogenerators: from technological progress to commercial applications, ACS Nano 17 (2023) 11087–11219.
[5] Z.L. Wang, Catch wave power in floating nets, Nature 542 (2017) 159–160.
[6] H. Wang, L. Xu, Z.L. Wang, Advances of high-performance triboelectric nanogenerators for blue energy harvesting, Nanoenergy Adv. 1 (2021) 32–57.
[7] X. Li, L. Xu, P. Lin, X. Yang, H. Wang, H. Qin, Z.L. Wang, Three-dimensional chiral networks of triboelectric nanogenerators as inspired by metamaterial's structure, Energy Environ. Sci. (2023), https://doi.org/10.1039/D3EE01035J.
[8] J. Bae, J. Lee, S. Kim, J. Ha, B.S. Lee, Y. Park, C. Choong, J.B. Kim, Z.L. Wang, H. Y. Kim, J.J. Park, U.I. Chung, Flutter-driven triboelectrification for harvesting wind energy, Nat. Commun. 5 (2014) 4929.
[9] W. Xu, H. Zheng, Y. Liu, X. Zhou, C. Zhang, Y. Song, X. Deng, M. Leung, Z. Yang, R. X. Xu, Z.L. Wang, X.C. Zeng, Z. Wang, A droplet-based electricity generator with high instantaneous power density, Nature 578 (2020) 392–396.
[10] S. Niu, X. Wang, F. Yi, Y.S. Zhou, Z.L. Wang, A universal self-charging system driven by random biomechanical energy for sustainable operation of mobile electronics, Nat. Commun. 6 (2015) 8975.
[11] Z.L. Wang, Triboelectric nanogenerator (TENG)-sparking an energy and sensor revolution, Adv. Energy Mater. 10 (2020) 2000137.
[12] S. Niu, Z.L. Wang, Theoretical systems of triboelectric nanogenerators, Nano Energy 14 (2015) 161–192.
[13] L. Xu, T.Z. Bu, X.D. Yang, C. Zhang, Z.L. Wang, Ultrahigh charge density realized by charge pumping at ambient conditions for triboelectric nanogenerators, Nano Energy 49 (2018) 625–633.
[14] H. Wang, L. Xu, Y. Bai, Z.L. Wang, Pumping up the charge density of a triboelectric nanogenerator by charge-shuttling, Nat. Commun. 11 (2020) 4203.
[15] J. Wu, Y. Xi, Y. Shi, Toward wear-resistive, highly durable and high performance triboelectric nanogenerator through interface liquid lubrication, Nano Energy 72 (2020), 104659.
[16] S. Niu, S. Wang, L. Lin, Y. Liu, Y.S. Zhou, Y. Hu, Z.L. Wang, Theoretical study of contact-mode triboelectric nanogenerators as an effective power source, Energy Environ. Sci. 6 (2013) 3576–3583.
[17] J. Wang, C. Wu, Y. Dai, Z. Zhao, A. Wang, T. Zhang, Z.L. Wang, Achieving ultrahigh triboelectric charge density for efficient energy harvesting, Nat. Commun. 8 (2017) 88.
[18] K. Wang, J. Li, J. Li, C. Wu, S. Yi, Y. Liu, J. Luo, Hexadecane-containing sandwich structure based triboelectric nanogenerator with remarkable performance enhancement, Nano Energy 87 (2021), 106198.
[19] W. He, W. Liu, S. Fu, H. Wu, C. Shan, Z. Wang, Y. Xi, X. Wang, H. Guo, H. Liu, C. Hu, Ultrahigh performance triboelectric nanogenerator enabled by charge transmission in interfacial lubrication and potential decentralization design, Research 2022 (2022) 9812865.
[20] L. Zhou, D. Liu, Z. Zhao, S. Li, Y. Liu, L. Liu, Y. Gao, Z.L. Wang, J. Wang, Simultaneously enhancing power density and durability of sliding-mode triboelectric nanogenerator via interface liquid lubrication, Adv. Energy Mater. 10 (2020) 2002920.
[21] V. Nguyen, R. Yang, Effect of humidity and pressure on the triboelectric nanogenerator, Nano Energy 2 (2013) 604–608.
[22] H. Qin, L. Xu, S. Lin, F. Zhan, K. Dong, K. Han, H. Wang, Y. Feng, Z.L. Wang, Underwater energy harvesting and sensing by sweeping out the charges in an electric double layer using an oil droplet, Adv. Funct. Mater. 32 (2022) 2111662.
[23] C. Xu, Y. Zi, A.C. Wang, H. Zou, Y. Dai, X. He, P. Wang, Y.C. Wang, P. Feng, D. Li, Z. L. Wang, On the electron-transfer mechanism in the contact-electrification effect, Adv. Mater. 30 (2018), e1706790.

[24] S. Lin, L. Xu, L. Zhu, X. Chen, Z.L. Wang, Electron transfer in nanoscale contact electrification: photon excitation effect, Adv. Mater. 31 (2019), e1901418.
[25] S. Lin, L. Xu, A.C. Wang, Z.L. Wang, Quantifying electron-transfer in liquid-solid contact electrification and the formation of electric double-layer, Nat. Commun. 11 (2020) 399.
[26] S. Niu, Y. Liu, S. Wang, L. Lin, Y.S. Zhou, Y. Hu, Z.L. Wang, Theoretical investigation and structural optimization of single-electrode triboelectric nanogenerators, Adv. Funct. Mater. 24 (2014) 3332–3340.
[27] F. Zhan, A.C. Wang, L. Xu, S. Lin, J. Shao, X. Chen, Z.L. Wang, Electron transfer as a liquid droplet contacting a polymer surface, ACS Nano 14 (2020) 17565–17573.
[28] S. Lin, Z.L. Wang, Scanning triboelectric nanogenerator as a nanoscale probe for measuring local surface charge density on a dielectric film, Appl. Phys. Lett. 118 (2021), 193901.
[29] J. Nie, Z. Ren, L. Xu, S. Lin, F. Zhan, X. Chen, Z.L. Wang, Probing contact-electrification-induced electron and ion transfers at a liquid-solid interface, Adv. Mater. 32 (2020), e1905696.
[30] Z.H. Lin, G. Cheng, S. Lee, K.C. Pradel, Z.L. Wang, Harvesting water drop energy by a sequential contact-electrification and electrostatic-induction process, Adv. Mater. 26 (2014) 4690–4696.
[31] Y.S. Zhou, Y. Liu, G. Zhu, Z.H. Lin, C.F. Pan, Q.S. Jing, Z.L. Wang, In situ quantitative study of nanoscale triboelectrification and patterning, Nano Lett. 13 (2013) 2771–2776.
[32] S. Lin, L. Xu, C. Xu, X. Chen, A.C. Wang, B. Zhang, P. Lin, Y. Yang, H. Zhao, Z. L. Wang, Electron transfer in nanoscale contact electrification: effect of temperature in the metal-dielectric case, Adv. Mater. 31 (2019), e1808197.
[33] V.M. Gun'ko, V.I. Zarko, E.V. Goncharuk, L.S. Andriyko, V.V. Turov, Y. M. Nychiporuk, R. Leboda, J. Skubiszewska-Zieba, A.L. Gabchak, V.D. Osovskii, Y. G. Ptushinskii, G.R. Yurchenko, O.A. Mishchuk, P.P. Gorbik, P. Pissis, J.P. Blitz, TSDC spectroscopy of relaxational and interfacial phenomena, Adv. Colloid Interfac. 131 (2007) 1–89.
[34] L. Yang, J. Ho, E. Allahyarov, R. Mu, L. Zhu, Semicrystalline structure dielectric property relationship and electrical conduction in a biaxially oriented poly (vinylidene fluoride) film under high electric fields and high temperatures, ACS Appl. Mater. Interfaces 7 (2015) 19894–19905.
[35] J. Hillenbrand, N. Behrendt, V. Altstädt, H.W. Schmidt, G.M. Sessler, Electret properties of biaxially stretched polypropylene films containing various additives, J. Phys. D: Appl. Phys. 39 (2006) 535–540.
[36] R. Chen, Y. Kirsh, thermally stimulated processes, Pergamon Press, Oxford, Analysis (1981).

Huaifang Qin received his M.S. degree from Henan University in 2019. He is currently pursuing the Ph.D. degree in Beijing Institute of Nanoenergy and Nanosystems, Chinese Academy of Sciences, China. His current research interests include contact-electrification and underwater energy harvesting.

Prof. Liang Xu received his Ph.D. degree from Tsinghua University (THU) in 2012. He is now a professor and principal investigator in Beijing Institute of Nanoenergy and Nanosystems, Chinese Academy of Sciences (CAS). His research interests include flexible electronics, soft robotics, nanogenerators and self-powered nanosystems, ocean energy harvesting, fundamental tribological phenomena, scanning probe microscopy and molecular dynamics simulation.

Dr. Fei Zhan received her Ph.D. degree in Chemical Technology from Dalian University of Technology. She has been a postdoctoral fellow in Zhong Lin Wang's group at Beijing Institute of Nanoenergy and Nanosystems, and is currently an assistant professor at Beijing University of Chemical Technology. Her research interests mainly focus on liquid-solid interface and carbon-based materials. She has presided 5 research projects.

Prof. Zhong Lin (ZL) Wang received his Ph.D. from Arizona State University in physics. He is now the director of Beijing Institute of Nanoenergy and Nanosystems. Prof. Wang has made original and innovative contributions to the synthesis, discovery, characterization and understanding of fundamental physical properties of oxide nanobelts and nanowires, as well as applications of nanowires in energy sciences, electronics, optoelectronics and biological science. His discovery and breakthroughs in developing nanogenerators established the principle and technological road map for harvesting mechanical energy from environment and biological systems for powering personal electronics. His research on self-powered nanosystems has inspired the worldwide effort in academia and industry for studying energy for micro-nano-systems, which is now a distinct disciplinary in energy research and future sensor networks. He coined and pioneered the field of piezotronics and piezophototronics by introducing piezoelectric potential gated charge transport process in fabricating new electronic and optoelectronic devices. Details can be found at: www.nanoscience.gatech.edu.